Interaction Between the Thyroarytenoid and Lateral Cricoarytenoid Muscles in the Control of Vocal Fold Adduction and Eigenfrequencies

Jun Yin[1]
Speech Production Laboratory,
Department of Head and Neck Surgery,
University of California, Los Angeles,
31-24 Rehabilitation Center,
1000 Veteran Avenue,
Los Angeles, CA 90095-1794

Zhaoyan Zhang[2]
Speech Production Laboratory,
Department of Head and Neck Surgery,
University of California, Los Angeles,
31-24 Rehabilitation Center,
1000 Veteran Avenue,
Los Angeles, CA 90095-1794
e-mail: zyzhang@ucla.edu

Although it is known vocal fold adduction is achieved through laryngeal muscle activation, it is still unclear how interaction between individual laryngeal muscle activations affects vocal fold adduction and vocal fold stiffness, both of which are important factors determining vocal fold vibration and the resulting voice quality. In this study, a three-dimensional (3D) finite element model was developed to investigate vocal fold adduction and changes in vocal fold eigenfrequencies due to the interaction between the lateral cricoarytenoid (LCA) and thyroarytenoid (TA) muscles. The results showed that LCA contraction led to a medial and downward rocking motion of the arytenoid cartilage in the coronal plane about the long axis of the cricoid cartilage facet, which adducted the posterior portion of the glottis but had little influence on vocal fold eigenfrequencies. In contrast, TA activation caused a medial rotation of the vocal folds toward the glottal midline, resulting in adduction of the anterior portion of the glottis and significant increase in vocal fold eigenfrequencies. This vocal fold-stiffening effect of TA activation also reduced the posterior adductory effect of LCA activation. The implications of the results for phonation control are discussed. [DOI: 10.1115/1.4028428]

Keywords: vocal fold adduction, muscle activation, thyroarytenoid, lateral cricoarytenoid

1 Introduction

A prerequisite for phonation is vocal fold adduction or approximation of the two vocal folds to close the glottis (the airspace between the two folds), which enhances the glottal fluid–structure interaction and induces the vocal folds into a self-sustained vibration. The resulting vibration pattern and consequently the produced voice depend on the geometry and stiffness conditions of the adducted vocal folds [1–3], with different vocal fold posturing producing different voice types [4–7]. Understanding the muscular control mechanisms of vocal fold adduction and the stiffness and stress consequence of different adductory patterns is critical to understanding how humans are able to produce a variety of voice types.

It is generally assumed that vocal fold adduction is achieved primarily through motion of the arytenoid cartilages due to activation of the LCA and the interarytenoid (IA) muscles. The vocal folds are layered soft tissue structures that attach anteriorly to the thyroid cartilage and posteriorly to the arytenoid cartilages (Fig. 1(*a*)). The arytenoid cartilages sit on the upper posterior border of the cricoid cartilage, forming the cricoarytenoid joint (CAJ), which is a synovial joint of the ball-and-socket type [8]. The LCA muscles run between the muscular process of the arytenoid cartilage and the side of the cricoid cartilage, and the IA muscles attach to the muscular processes of the two arytenoid cartilages. Contraction of both muscles is generally considered to adduct the arytenoid cartilages and approximate the two vocal folds. Another muscle, the posterior cricoarytenoid (PCA) muscle (not shown in Fig. 1), also attaches to the arytenoid but its contraction abducts the arytenoid cartilages and opens the glottis. In addition to these three muscles, previous studies [9,10] showed that the TA muscle also plays an important role in anterior vocal fold adduction. The TA muscle originates from the thyroid cartilage and inserts into the anterolateral surface of the arytenoid cartilages and forms the main body of the vocal folds. Choi et al. [10] showed that contraction of the LCA/IA alone closed the cartilaginous portion of the glottis (the portion between the vocal processes of the arytenoid cartilages and the posterior commissure) but left an opening in the membranous portion (the portion between the anterior commissure and the vocal processes of the arytenoid cartilages) of the glottis (Fig. 1(*c*)), whereas TA muscle contraction completely closed the anterior glottis (Fig. 1(*d*)). Similar observation was also reported in a more recent study by Chhetri et al. [9].

Despite these general observations, the interaction between the LCA/IA/TA muscles in the control of vocal fold adduction has never been systematically investigated. Furthermore, it remains essentially unknown how the stiffness and stress conditions within the vocal folds change with different vocal fold adductory patterns, due to the lack of reliable techniques for in vivo measurement of the stiffness and stress within the vocal folds (in both animal models or live humans). Inference of changes in stiffness from vocal fold deformation is also difficult because in vivo observation of the motion of the arytenoid cartilages and the vocal folds is limited to an endoscopic superior view, which can be misleading. For example, although the arytenoid cartilage motion

[1]Present address: Department of Mechanics and Engineering Science, Fudan University, Shanghai, China.
[2]Corresponding author.
Manuscript received March 24, 2014; final manuscript received August 5, 2014; accepted manuscript posted August 28, 2014; published online September 11, 2014. Assoc. Editor: Jonathan Vande Geest.

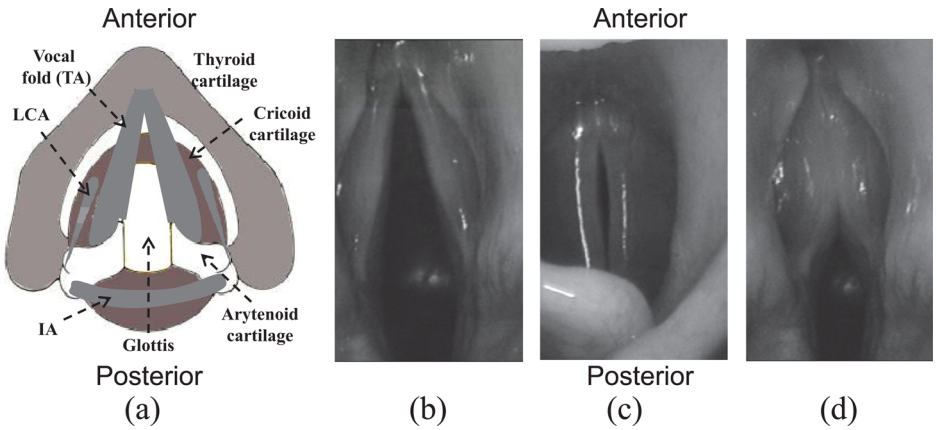

Fig. 1 (*a*) A sketch of the laryngeal framework including the vocal fold, the thyroid, cricoid, and arytenoid cartilages, and the LCA and IA muscles from a superior view. (*b*) Superior view of a canine larynx at resting (respiratory) position. (*c*) LCA activation adducts the glottis but leaves a gap in the middle-membranous glottis. (*d*) TA activation completely closes the anterior glottis but leaves a large gap at the posterior glottis. Figures (*b*)–(*d*) are images obtained from in vivo canine larynx experiments in Choi et al. (1993).

appears to be a "pivoting" rotation about a vertical axis (an axis perpendicular to the cricoid facet) from an endoscopic view, anatomical studies suggested that this pivoting rotational motion along a vertical axis may be restricted by the cricoid–arytenoid cartilage interaction in the CAJ, and the arytenoid cartilage motion may be limited to either a translational sliding motion and/or a rigid-body rocking motion (rotation in the coronal plane) along the long axis of the cricoid facet [11–16]. In fact, the exact arytenoid motion during vocal fold adduction, due to either LCA or TA activation, is still debatable.

Due to these experimental difficulties, numerical models of vocal fold adduction have been developed in previous studies e.g., Refs. [17–20] However, because of the highly nonlinear nature of muscle activation and vocal fold deformation, the interactions within the CAJ and its interaction with muscle activation were often not modeled in these studies and motion of the arytenoid cartilages was either imposed or constrained along a predefined rocking–sliding axis so that the interaction between the arytenoid and cricoid cartilages in the CAJ and its influence on arytenoid cartilage motion was not investigated. More importantly, because these previous models often assumed a rigid-body motion of the vocal folds, the induced vocal fold tissue deformation and changes in stress distribution within the vocal fold were thus not studied.

The goal of this study was to investigate the interaction between laryngeal muscles in determining arytenoid cartilage motion, the resulting adductory pattern, and changes in the stiffness condition within the vocal fold. Specifically, this study focused on the interaction between the LCA and the TA muscles, the two primary adductory muscles responsible for adduction of the membranous portion of the glottis. Inclusion of the IA muscle, which is generally assumed to be responsible for adduction of the cartilaginous glottis, significantly increases the complexity of the model and the number of interaction conditions to be investigated, and was thus not considered in this study. A 3D finite element model of the CAJ was developed in the commercial software COMSOL, using realistic geometry of the CAJ obtained from a MRI study [21,13]. Arytenoid cartilage motion and vocal fold deformation were investigated for different LCA/TA activation conditions. Since phonation onset occurs as two or more vocal fold eigenmodes are synchronized by the glottal flow and the resulting vocal fold vibration pattern was critically dependent on the vibration pattern in the vocal fold eigenmodes that are synchronized [22–25], the first ten in vacuo eigenfrequencies of the vocal fold at different conditions of LCA/TA activation were studied to understand the influence of vocal fold adduction on vocal fold vibration.

2 Model

2.1 Geometry and Boundary Conditions. The 3D finite element model included the vocal fold (with TA as the main component, see below), the LCA muscle, the arytenoid cartilage, and the cricoid cartilage (Fig. 2). The IA and PCA muscles (not shown in Fig. 2) were also included but not activated in this study. For simplicity, left–right symmetry in motion about the glottal midline was assumed so that only one vocal fold and one arytenoid cartilage were modeled in this study. The geometry of the arytenoid and cricoid cartilages was obtained from the computer solid model developed in Hunter and Thomson [21] based on the original magnetic resonance images (MRI) of a human laryngeal cartilage by Selbie et al.[13,14]. Note that the curves on the surface of the cartilages in Fig. 2 represent the curved surface of the cartilages, not the actual meshes used in the simulations. In this study, the cricoid cartilage was fixed. The interface between the arytenoid and cricoid cartilages at the CAJ was modeled as a "contact-sliding" interface, which allowed relative sliding motion between the two cartilages in the tangential direction along the interface. To simulate the effects of the covering soft tissues within the synovial CAJ, a virtual elastic film (Young's modulus of 100 kPa) was further added in between the two cartilages. The Young's modulus of this virtual elastic film was determined as the minimum value required to prevent large separation of the cartilages in the normal direction.

Because the original MRI data do not include any information that allows us to separate the different layers of soft tissue and the muscles, a body-cover two-layer simplified vocal fold with a uniform cross-sectional geometry along the anterior–posterior (AP) direction (Fig. 2(*c*)) was used, with the body layer consisting entirely of the TA muscle [4,23]. Similar simplified vocal fold geometry has been widely used in previous phonation studies [26–30,23,31]. The resting position of the vocal fold formed an initial glottal opening angle $\theta_0 = 13$ deg (Fig. 2(*a*)), which is within the human range as measured by Eckel and Sittel [32]. The vocal fold attached anteriorly to the thyroid cartilage, which was modeled as a fixed boundary condition to the anterior surface of the vocal folds, and posteriorly connected to the anterolateral surface of the arytenoid cartilage through a transitional layer (simulating the macular flava) (Fig. 2(*b*)). In humans, the vocal fold connects laterally to the thyroid cartilage through a soft tissue layer in the paraglottic space. In this study, this soft tissue layer was modeled as a spring foundation attached to the lateral surface of the vocal fold. Since no data existed for the material properties of this soft tissue layer, different spring constants in the range

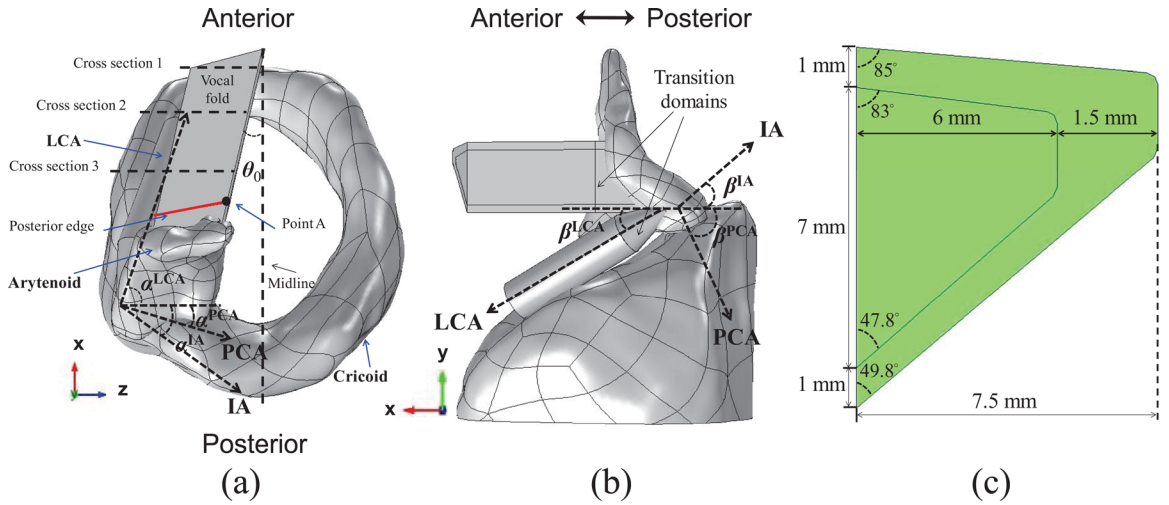

Fig. 2 A sketch of the computational model from (*a*) a top view and (*b*) a side view, and (*c*) the cross section of the vocal fold model. Note that the curves on the surface of the cartilages represent the curved surface of the cartilages, not the actual meshes used in the simulations. Figure 2(*a*) also defines a point A located at the medial posterior corner of the superior surface, a line located at the posterior edge on the superior surface of the vocal fold, and three coronal cross sections, the results on which are shown in Figs. 4, 5, and 7.

10^4–10^7 N/m^3 were tested and it was found that large values of the spring constant restricted vocal fold adduction. In the following, a spring constant $k_f = 10^4$ N/m^3 was used which did not significantly restrict the motion of the vocal folds.

Due to the lack of detailed geometric data of the LCA muscle, the LCA muscle was modeled as a cylinder that attached posteriorly to the muscular process of the arytenoid cartilage through a transition layer (Fig. 2(*b*)). In humans, the LCA muscle inserts anteriorly into the cricoid cartilage. For simplicity, a fixed boundary condition was applied to the anterior surface of the LCA muscle. Although the PCA and IA muscles were not activated in this study, the passive reaction forces generated by elongation or shortening of IA and PCA muscles due to arytenoid motion were calculated and applied as point forces to the muscular process of the arytenoid cartilage along the predefined muscle fiber directions (Fig. 2(*a*)), as described in Sec. 2.2. The muscle fiber directions, initial lengths, and initial cross-sectional areas of LCA, PCA, and IA muscles were based on measurements in Mineck et al. [33] and are listed in Table 1.

2.2 Material Properties. The cartilages are generally much stiffer than the vocal fold. In this study, both the arytenoid and cricoid cartilages were modeled as a linear elastic material with a very large Young's modulus of 50 MPa, which was slightly higher than that used in Hunter et al. [19]. The transition layers between cartilages and the vocal fold and the LCA muscle were modeled similarly as a linear elastic material but with a reduced Young's modulus of 5 MPa.

The vocal fold (including the TA muscle as the body layer), and the LCA, PCA, and IA muscles were modeled as hyperelastic materials. Similar to skeletal muscles [34,35], the strain energy function used in this study had both a passive and an active component,

$$W = W_{\text{passive}} + W_{\text{active}} \tag{1}$$

For the cover layer of the vocal fold, which was a passive soft tissue layer with no muscles, the strain energy function only had the passive component. A five-parameter Mooney–Rivlin model was used for the passive component, as in Yin and Zhang [36]

$$\begin{aligned} W_{\text{passive}} = {} & c_{10}(\bar{I}_1 - 3) + c_{01}(\bar{I}_2 - 3) \\ & + c_{20}(\bar{I}_1 - 3)^2 + c_{11}(\bar{I}_1 - 3)(\bar{I}_2 - 3) \\ & + c_{02}(\bar{I}_2 - 3)^2 + \frac{\kappa}{2}(J-1)^2 \end{aligned} \tag{2}$$

where $\bar{I}_1$ and $\bar{I}_2$ are the first and second modified principal invariants of the deformation tensor [37], J is the Jacobian or the volume ratio between the deformed and undeformed geometry, and the coefficients c and κ are model constants. For this study, both the vocal fold and the muscles were assumed nearly incompressible, with $\kappa = 3$ MPa. The other model coefficients in Eq. (2) were estimated by curve fitting the experimentally measured stress–strain curve of excised human larynges as reported in Zhang et al. [38] and are listed in Table 2.

The active component of the strain energy function was derived by considering a uniaxial motion due to the activation of an incompressible muscle fiber, in which case the active stress along the fiber direction is related to the fiber stretch as

$$\sigma_{\text{active}} = \lambda \frac{\partial W_{\text{active}}}{\partial \lambda} \tag{3}$$

Table 1 Anatomical properties of the LCA, PCA, IA muscles from Mineck et al. (2000)

Laryngeal muscles	Force direction angle α	Force direction angle β	Initial length (mm)	Initial cross sectional area (mm^2)
LCA	70 deg	30 deg	17	21.2
PCA	21.1 deg	71.4 deg	11.5	34.2
IA	41.6 deg	22.5 deg	9.4	12.1

Table 2 Model constants of the constitutive equations

	TA, cover layer	LCA, PCA, and IA
c_{10}	5×10^3 Pa	5×10^3 Pa
c_{01}	-3×10^3 Pa	-3×10^3 Pa
c_{11}	-2×10^4 Pa	-1×10^4 Pa
c_{20}	8×10^4 Pa	9×10^4 Pa
c_{02}	-2×10^4 Pa	-1×10^4 Pa
K	3×10^6 Pa	3×10^6 Pa
$\sigma_{\max}$	10^5 Pa	10^5 Pa
λ_{ofl}	1.4	1.4

where λ is the muscle fiber stretch along the fiber direction. As this study focused on the steady-state vocal fold deformation, the active stress due to muscle activation was assumed to be independent of the strain rate and scale linearly with the muscle activation level α

$$\sigma_{\text{active}} = \alpha\sigma_{\max} f_{\text{active}} \frac{\lambda}{\lambda_{\text{opt}}} \tag{4}$$

where $\sigma_{\max}$ is the maximum activation stress, λ_{opt} is the optimal stretch of muscle fiber at which maximum active stress occurs, and f_{active} is the normalized function of muscle active force defined as [19,36,39]

$$f_{\text{active}} = \begin{cases} 1 - 4\left(1 - \dfrac{\lambda}{\lambda_{\text{opt}}}\right)^2, & 0.5\lambda_{\text{opt}} \le \lambda \le 1.4\lambda_{\text{opt}} \\ 0, & \text{otherwise} \end{cases} \tag{5}$$

The active component of strain energy function was obtained by substituting Eqs. (4) and (5) into Eq. (3)

$$W_{\text{active}} = \begin{cases} \dfrac{\alpha\sigma_{\max}}{3}\left[4\left(1 - \dfrac{\lambda}{\lambda_{\text{opt}}}\right)^2 - 3\right]\left(1 - \dfrac{\lambda}{\lambda_{\text{opt}}}\right), & 0.5\lambda_{\text{opt}} \le \lambda \le 1.4\lambda_{\text{opt}} \\ 0, & \text{otherwise} \end{cases} \tag{6}$$

The value of λ_{opt} was set to 1.4 as in Blemker et al. [39], and the value for $\sigma_{\max}$ was taken from measurements from canine experiments in Alipour-Haghighi et al. [40]. All the model coefficients in Eqs. (2) and (6) are listed in Table 2.

For the passive force of the IA and PCA muscles, the individual muscle stretch due to arytenoid cartilage motion was first calculated, which was then used to calculate the corresponding stress using the passive strain energy function as defined in Eq. (2). The passive forces were then calculated by multiplying the passive stress by the cross-sectional area of the corresponding muscle, similar to Hunter et al.[19] and Yin and Zhang [36].

2.3 Model Implementation. The model was implemented in the commercial software Comsol. Simulations were performed using gradually refined meshes and mesh density convergence was considered reached when the difference in the predicted vocal fold displacement was within 5% between two consecutive meshes. For the results reported below, the model contained a total of 77,504 elements.

2.4 Model Validation and Comparison to Experiments. Direct validation of our model by comparing to experiments requires simultaneous measurement of the 3D vocal fold deformation and the stiffness and stress conditions within the vocal folds when the LCA and TA muscles are stimulated, either in human subjects or in vivo models (e.g., Berke et al., [41]). Neither of these measurements is possible at present. The lack of reliable techniques for in vivo measurement of vocal fold geometry and material properties also indicates that we have to estimate the input parameters to the numerical model, thus preventing a direct quantitative comparison to experiments.

As far as we know, the only available experimental data in the literature regarding laryngeal muscle stimulation are the in vivo canine experiments by Choi et al. [10] and Chhetri et al. [9] in which endoscopic images of vocal fold adduction in a superior view were recorded at conditions of individual muscle activation, as shown in Figs. 1(*b*)–1(*d*). In this study, model validation was thus limited to qualitative comparison of the vocal fold adduction pattern between the model predictions and the endoscopic observations of changes in glottal opening and shape in these two studies. Figures 3(*a*) and 3(*e*) show the predicted glottis profiles (i.e., the edge of the glottis when viewed from above) when the LCA muscle and the TA muscle was fully activated alone (i.e., with all other muscles inactive), respectively. Also shown is the glottal profile at the resting condition without muscle activation (thin lines). Full LCA activation completely closed the posterior portion of the glottis but left a small gap in the anterior portion of the glottis, whereas full TA activation completely closed the anterior portion of the glottis but there was a large gap in the posterior glottis. Comparing Figs. 3(*a*) and 3(*e*) to Figs. 1(*b*)–1(*d*), these observations are consistent with the observations in the in vivo experiments in Choi et al. [10] and Chhetri et al. [9] (Fig. 1). Considering the lack of accurate data regarding the material properties and geometry of the vocal folds and the LCA/TA muscles, this qualitative agreement between experimental observations and our model predictions suggests that this model was adequate for a qualitative study of muscular control of vocal fold adduction.

3 Results

3.1 Vocal Fold Motion Due to LCA Activation. Figures 3(*b*)–3(*d*) show the deformation of the model in three different views when the LCA muscle alone was fully activated ($\alpha_{\text{LCA}} = 1$, $\alpha_{\text{TA}} = 0$). (Figs. 3(*f*)–3(*h*) show the deformation due to TA muscle activation which are discussed in Sec. 3.2.) The outline of the undeformed geometry of the model was also shown in the figure. The top view in Fig. 3(*b*) shows a medial motion of the arytenoid cartilage which closed the posterior portion of the glottis. The side view in Fig. 3(*c*) shows a downward motion of the arytenoid and a downward bending motion of the posterior half of the vocal fold. The frontal view in Fig. 3(*d*) shows a strong inward (medial) rocking motion of the arytenoid cartilage about the cricoid cartilage. To further quantify the arytenoid motion and its rotation axis, Fig. 4 shows the displacement of a point located at the medial–posterior corner of the superior surface of the vocal fold (labeled as "A" in Fig. 2(*a*)) and the rotational angles of the posterior edge of the superior surface of the vocal fold in both the coronal plane (*y*-*z* plane) and the horizontal plane (*x*-*z* plane), as a function of LCA activation (other muscles are set as zero activation). Figure 4(*a*) shows that LCA activation caused point A to move downward and medially. The displacement along the AP direction was much smaller, indicating almost negligible shortening or elongation of the vocal fold. Figure 4(*b*) further shows that the rotation motion of the arytenoid was primarily a rocking motion in the coronal plane about the long axis of the cricoid facet, with a much smaller rotation or pivoting motion in the horizontal plane about a vertical axis, particularly at conditions of strong LCA activation. Thus, in this study, LCA activation led primarily to a rocking motion of the arytenoid in the coronal plane about the cricoid facet. Both the sliding motion and the rotational motion in the horizontal plane about a vertical axis were quite limited.

This rocking motion of the arytenoid led to a complex bending motion of the vocal fold, particularly at the posterior half of the vocal fold, as shown in Fig. 3(*b*). Figures 5(*a*)–5(*c*) show the deformation of three cross sections (anterior, middle, and posterior, as defined in Fig. 2(*a*)) of the vocal fold, with the color representing the distribution of the AP strain (ε_{xx}). Note that a negative AP strain indicates the cross section was compressed along the AP direction, whereas positive values indicate elongation along the AP direction. Figures 3 and 5 show that different parts of the vocal fold along the AP direction bent toward different directions: the anterior portion bent medially (Fig. 3(*b*); Fig. 5(*a*): more negative AP strain in the medial half than the lateral surface); the middle portion moved medially, started to rotate clockwise in the coronal plane, and bent downward (Figs. 3(*c*) and 5(*b*); and the posterior portion showed both large medial movement and rotation in the coronal plane, and bent laterally (Figs. 3(*b*) and 5(*c*): positive AP

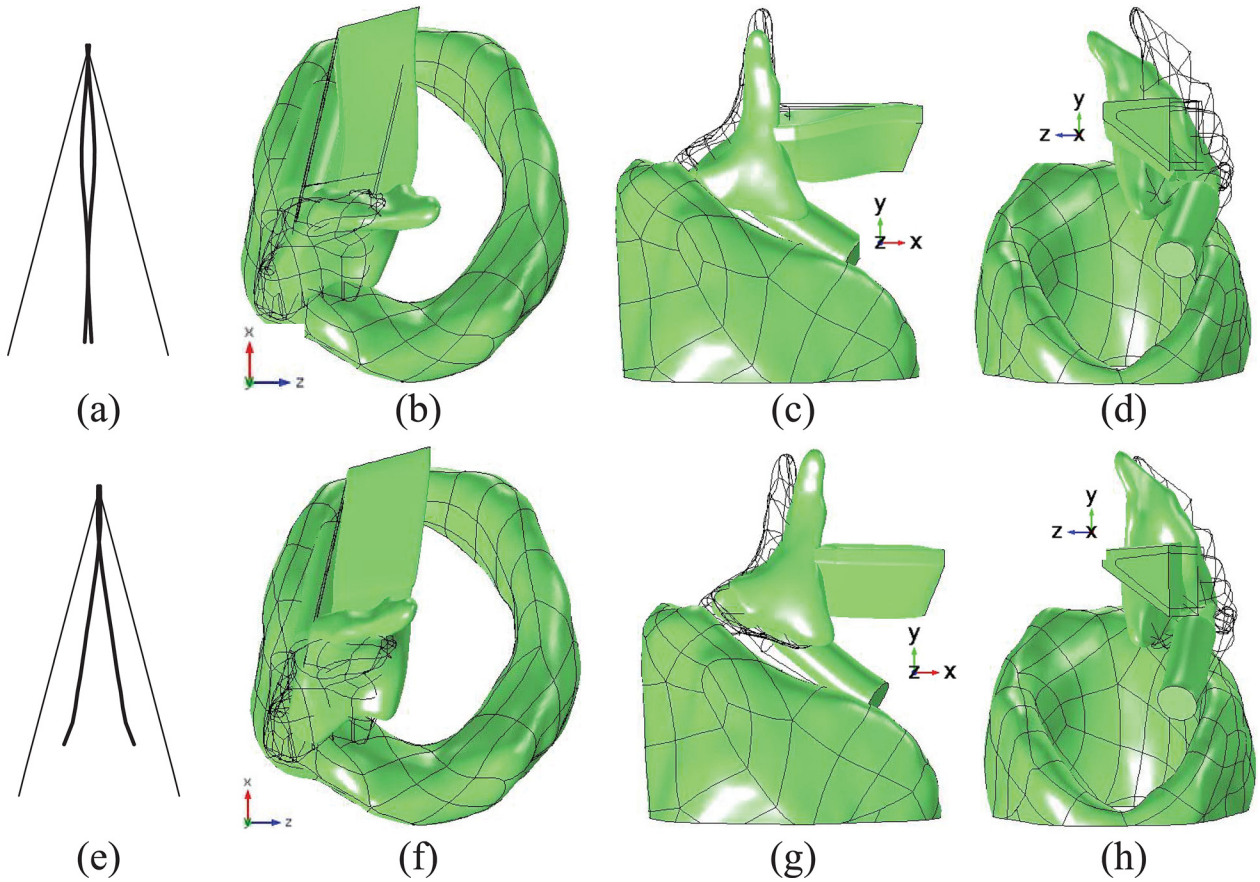

Fig. 3 The glottal shape (*a,e*) and the deformed model in a top view (*b,f*), side view (*c,g*), and frontal view (*d,h*) under the condition of full LCA activation alone (top) and full TA activation alone (bottom). The thin lines indicate the original glottal shape or geometry. Note that the curves on the surface of the cartilages represent the curved surface of the cartilages, not the actual meshes used in the simulations.

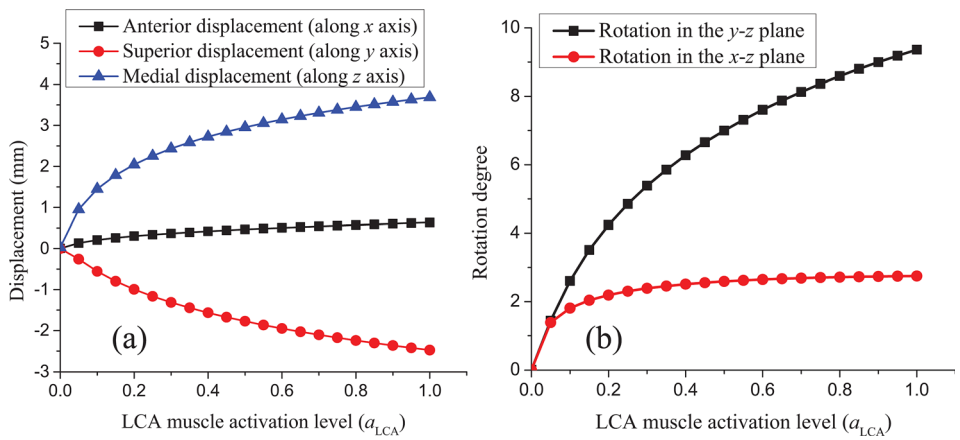

Fig. 4 (*a*) The three components of the displacement of point A as a function of the LCA activation level. (*b*) The rotation angles of the posterior edge in the coronal plane and the horizontal plane as a function of the LCA activation level. The point A and the posterior edge were defined in Fig. 2(*a*).

strain in the medial half and negative in the lateral half). Due to this complex bending motion, the vocal fold formed a convex glottis at the posterior part to adduct the posterior end, but a concave glottis at the anterior portion (Figs, 3(*a*) and 3(*b*)). As a result, LCA activation was able to close the posterior glottis but left a small gap in the anterior portion of the glottis.

Note that, although the PCA and IA muscles were not activated in this study, it was found that the passive forces from the PCA and IA muscles in response to arytenoid cartilage motion were essential to producing the rocking motion of the arytenoid cartilage. As shown in Fig. 6, without such passive forces from the PCA and IA muscles, no obvious medial displacement was observed even when the LCA muscle was maximally activated (Fig. 6(*a*)), and contraction of LCA muscle only led to a downward sliding motion of the arytenoid cartilage along the cricoid cartilage (Fig. 6(*b*)).

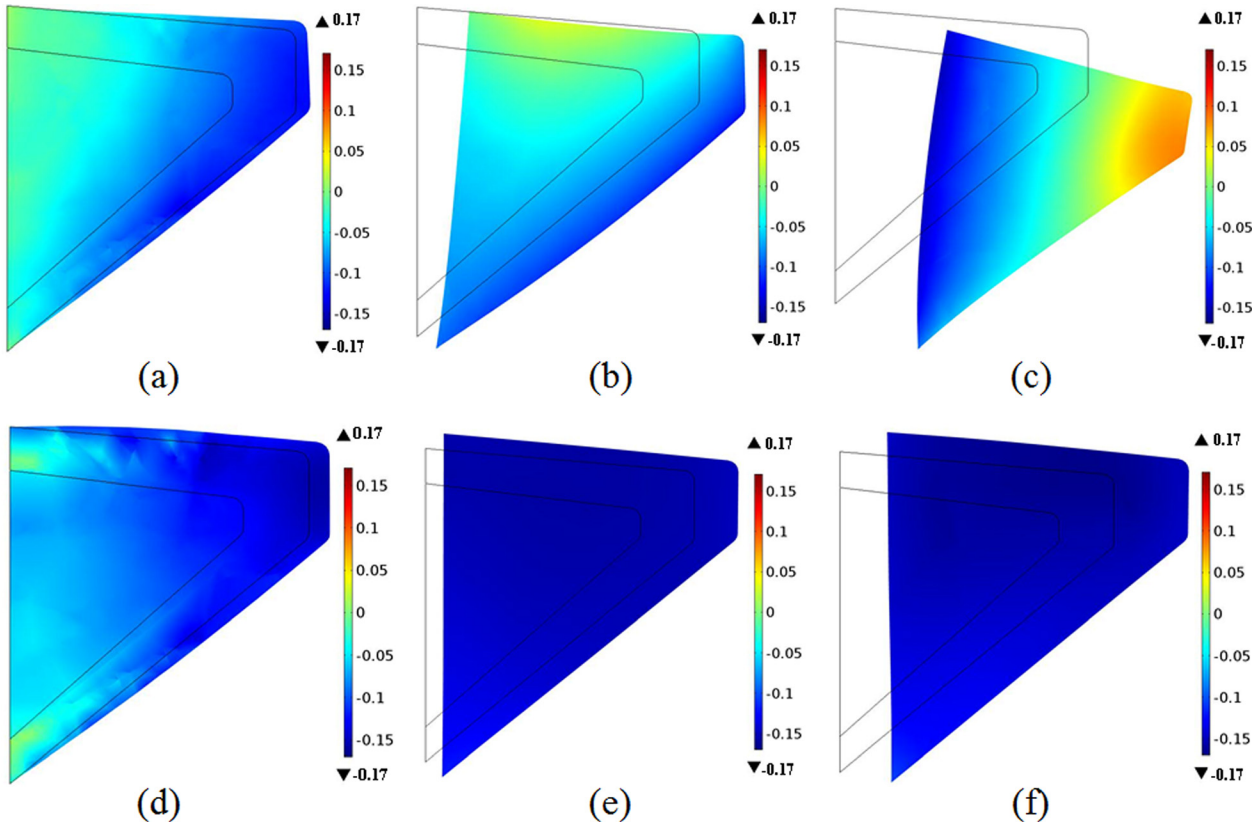

Fig. 5 The deformed geometry of the anterior (left), middle (middle), and posterior (right) cross sections of the vocal fold at the condition of full LCA activation alone (top) and full TA activation alone (bottom). The solid lines indicate the undeformed geometry of the body and cover layer. The three cross sections are defined in Fig. 2(*a*). The color within the cross sections represents the AP Strain ε_{xx}.

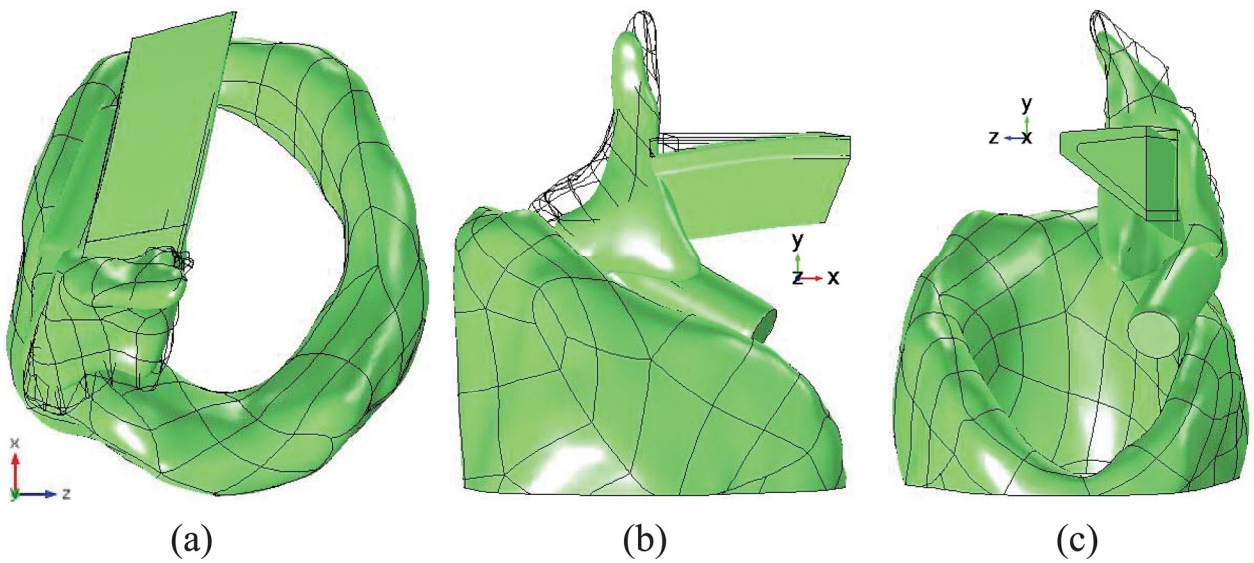

Fig. 6 Model deformation in a top view (*a*), side view (*b*), and frontal view (*c*) under full LCA activation but without considering the passive forces of PCA and IA muscles

3.2 Vocal Fold Motion Due to TA Activation. Figures 3(*f*)–3(*h*) show the motion of the arytenoid cartilage and the vocal fold when the TA muscle was fully activated alone. TA contraction shortened the vocal fold, which pulled the arytenoid cartilage to rotate forward about the long axis of the cricoid cartilage (Fig. 3(*g*)). Unlike the complex bending motion of the vocal fold in the case of LCA activation, the resulting vocal fold motion in this case was almost a whole-body uniform rotation around its anterior attachment to the thyroid cartilage toward the glottal centerline. Due to this whole-body medial rotation, the vocal fold edge along the AP length did not have the concave shape at the anterior portion as observed under LCA activation. Instead, the vocal fold edge had a slightly convex shape, because TA contraction also caused the vocal fold to bulge out toward the glottal midline

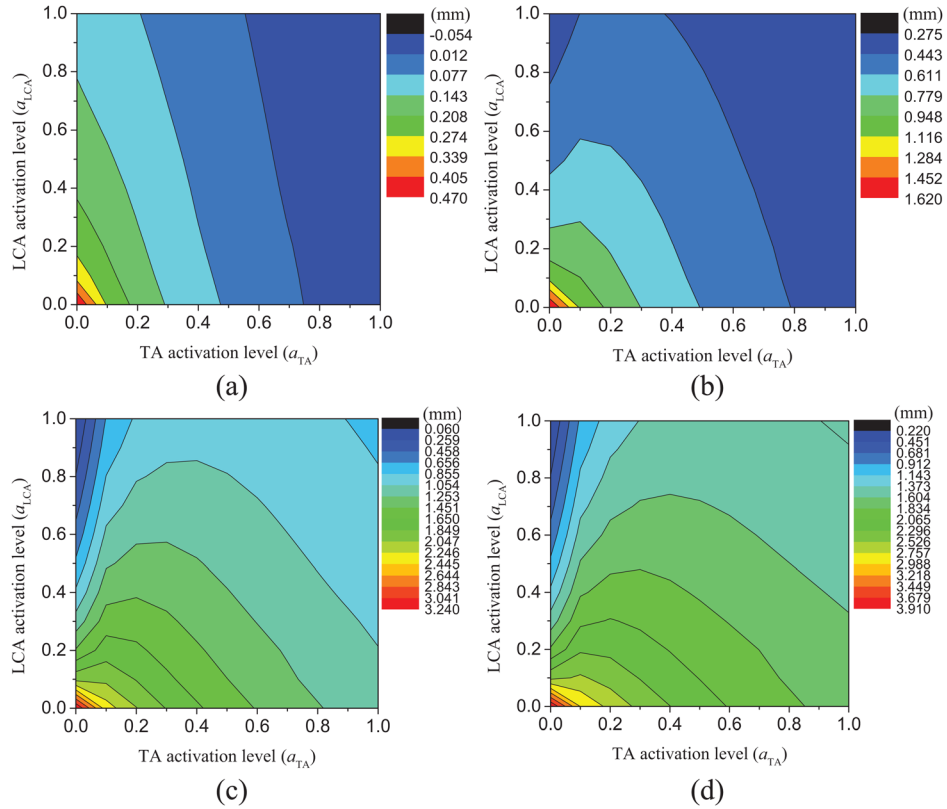

Fig. 7 Contours of the glottal width at locations of (*a*) cross section 1, (*b*) cross section 2, (*c*) cross section 3, and (*d*) the posterior edge of the superior surface of the vocal fold as a function of the LCA and TA activation levels

(Fig. 3(*f*)). As a result, TA contraction was able to completely close the anterior portion of the glottis (Fig. 3(*e*)). Posteriorly, due to the triangular shape of the original glottis, TA activation was unable to fully close the posterior portion of the glottis, despite the larger medial displacement at the posterior end of the vocal fold, as shown in Fig. 3. In this study, the maximum TA contraction led to an average strain of about −0.17, which is within the range observed in both experiments and simulations [40,42].

3.3 Interaction Between the LCA and TA Muscles. The interaction between the LCA and TA muscles in controlling glottal opening is illustrated in Fig. 7, which shows the contour plots of the glottal gap in three cross sections (anterior, middle, and posterior) and the posterior surface of the vocal fold (as defined in Fig. 2(*a*)) as a function of the LCA/TA activation levels. In the anterior portion (Fig. 7(*a*)), contraction of both muscles reduced the glottal gap. Control of the posterior glottal opening was more complex (Figs. 7(*b*)–7(*d*)). While increasing level of LCA activation always reduced the posterior glottal width, increasing TA activation first increased then decreased the posterior glottal width for medium to high levels of LCA activation. Thus, while TA activation was always adductory for the anterior glottis, its effect was adductory for the posterior portion of the glottis only for very low levels of LCA activation. At medium to high levels of LCA activation, TA activation actually abducted the posterior portion of the glottis.

3.4 Influence on Vocal Fold Eigenfrequencies. To understand how vocal fold adduction affects the stiffness condition within the vocal fold, a prestressed eigenvalue analysis, which takes into consideration of the static vocal fold deformation and stress due to muscle activation, was performed, as described in Yin and Zhang [36]. Figure 8 shows the contour plot of the first eigenfrequency as a function of the TA and LCA activation levels. The first eigenfrequency was largely determined by the TA activation level, as indicated by the vertical contour lines, except for conditions of very small TA activation levels ($a_{TA} < 0.2$) at which increasing LCA activation also led to a slight increase in the first eigenfrequency. Similar patterns can be observed regarding the influence of LCA/TA activation on higher-order eigenfrequencies, as shown in Fig. 9 for the first ten eigenfrequencies. For a given TA activation level (Figs. 9(*a*)–9(*c*)), increasing LCA activation had almost no influence on the first ten eigenfrequencies except for low TA activation levels (Fig. 9(*a*)). In contrast, increasing TA activation significantly increased the eigenfrequencies, for all levels of LCA activation. Considering that phonation results from

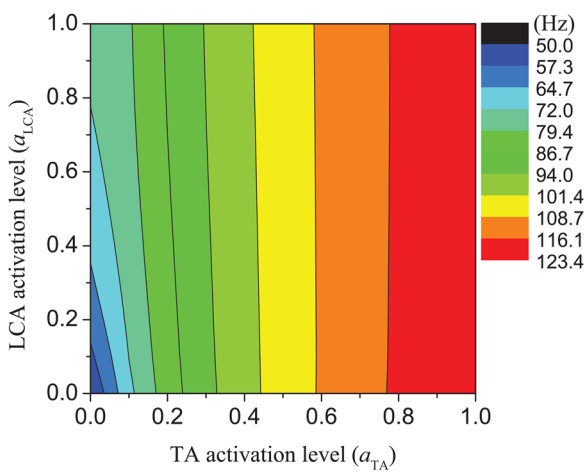

Fig. 8 Contour plot of the first vocal fold eigenfrequency as a function of the LCA and TA activation levels

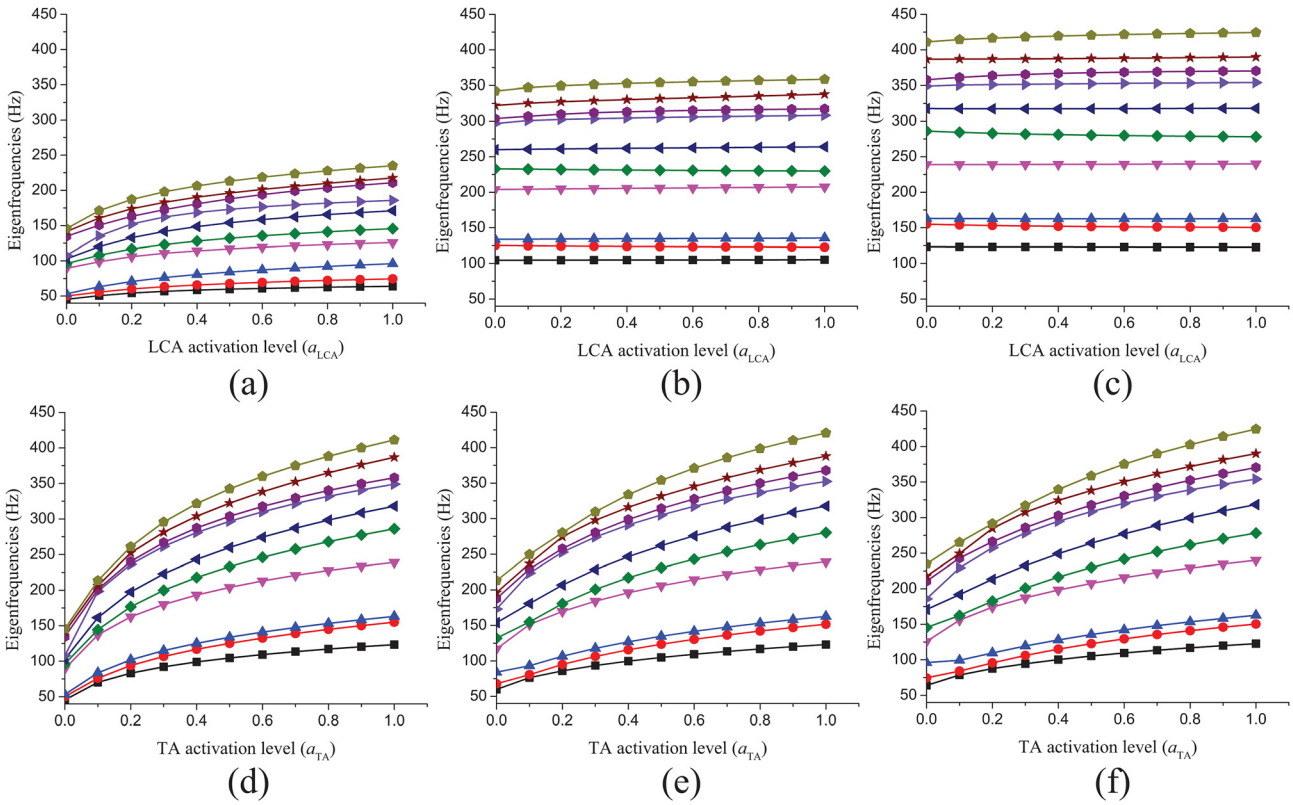

Fig. 9 The first ten eigenfrequencies of the vocal fold as a function of the LCA activation level for three levels of TA activation ((*a*): $\alpha_{TA} = 0$; (*b*): $\alpha_{TA} = 0.5$; and (*c*): $\alpha_{TA} = 1$) and as a function of the TA activation level for three levels of LCA activation ((*d*): $\alpha_{LCA} = 0$; (*e*): $\alpha_{LCA} = 0.5$; (*f*): $\alpha_{LCA} = 1$)

synchronization of the first few eigenmodes of the vocal folds, Fig. 9 suggests that LCA contraction is unlikely to have any noticeable influence on phonation frequency except for conditions of low TA activation. This observation is consistent with the experimental observation in Chhetri et al. [43], which showed that LCA activation led to only modest increase in phonation frequency.

4 Discussion

The movement of the arytenoid cartilage is determined by not only the forces exerted by muscle contraction, but also the constraints of the arytenoid cartilage within the CAJ. Previous numerical studies often constrained arytenoid cartilage motion to rotation about a prespecified "virtual axis". In the two-dimensional adduction model in Titze and Hunter [20], this virtual axis was set to be perpendicular to the transverse plane; while other 3D adduction models allowed the arytenoid cartilage to rotate around and slide along a fixed axis [17–19]. In the present study, using realistic geometry of the arytenoid and cricoid cartilages and without any predefined virtual axis, we showed that arytenoid cartilage motion under LCA activation was primarily a rocking motion about the cricoid facets in the coronal plane, confirming previous assessments based on quantitative anatomical measures [13,44]. Several factors are critical to achieving this rocking motion. One is the virtual elastic film in between the arytenoid and the cricoid cartilages (simulating the mucosa layer covering the cartilages) that prevented separation of the two cartilages in the normal direction and forced the arytenoid cartilage to be in close contact with the cricoid cartilage. This restriction prevented a large rotational motion about a vertical axis and limited arytenoid cartilage motion to a rocking motion around and/or a sliding motion along the cricoid cartilage. The forward-sliding motion of the arytenoid cartilage along the cricoid cartilage was further resisted by the passive forces of the PCA and IA muscles. As a result, the rocking motion became the least resisted motion of the arytenoid cartilage, as observed in Fig. 3.

This study also revealed a mechanism as to why LCA muscle activation was unable to close the anterior portion of the glottis. Vocal fold adduction under LCA activation was induced purely by arytenoid motion which only slightly stiffened the vocal fold. As a result, the rocking motion of the arytenoid cartilage was able to adduct or bend the vocal fold mostly at the posterior half but not much at the anterior portion.

Although it is generally assumed that TA contraction adducts the anterior portion due to medial bulge of the vocal fold, our study showed that, due to constraints of the CAJ, contraction of the TA muscle led to a medial rotation of the vocal fold toward the glottal midline. This medial rotation, together with a secondary contribution from vocal fold bulging due to TA muscle contraction, allowed TA contraction to completely closed the anterior portion of the glottis. However, this TA adduction was achieved through shortening and significant stiffening of the vocal folds, which resisted the rocking motion of the arytenoid cartilages due to LCA activation. As a result, TA contraction also had an abduction effect at the posterior membranous portion of the glottis for medium to high LCA activation levels, as shown in Fig. 7.

Although the rocking motion due to LCA activation led to complex bending deformation within the vocal folds, the overall effects of LCA activation on vocal fold stiffness were limited, as shown by the relatively small changes in vocal fold eigenfrequencies with increasing LCA activation. In contrast, TA activation led to a more uniform deformation within the vocal fold, i.e., vocal fold shortening, and thus had a much larger effect on vocal fold stiffness and eigenfrequencies. Previous studies [3,28] indicated that vocal fold stiffness rather than the degree of vocal fold approximation is more important in determining the glottal closure pattern during phonation, and that approximation of the vocal fold alone (without simultaneous stiffening) is insufficient in

achieving complete glottal closure during vibration. Considering the dominant effects of the TA muscle in relative to the LCA muscle in the control of both vocal fold adduction and eigenfrequencies, it seems that the TA muscle, instead of the LCA muscle, may play an important role in controlling the closed quotient (the fraction of the cycle the glottis is completely closed) of vocal fold vibration, which is essential to the production of the harmonic component of voice, and therefore may act as a fine controller of voice quality (e.g., variation from breathy, normal, to pressed voice quality).

The main limitation of this study lies in the accuracy (or inaccuracy) of the material properties of the vocal fold and the muscles used in our model. There have been little experimental data characterizing the nonlinear anisotropic material properties of the vocal folds and their spatial variations. Even less data are available on the material properties, both passive and active, of the individual laryngeal muscles involved. Large variability is also known to exist in these material properties across subjects. Due to this lack of reliable experimental data on material properties, numerical investigation of muscular control mechanisms of vocal fold posturing has to reply on assumptions or simplifications on the material properties of the laryngeal muscles, the cartilages, and the transition layers in between. However, efforts have been made in this study to base these model simplifications on the limited experimental data available. For example, the vocal fold constitutive model of this study was derived based on previous uniaxial tensile experiments. The maximum muscle activation stresses were based on previous tetanic muscle stimulation in canine experiments. Furthermore, the cross-sectional areas and orientations of the muscles involved were based on previous anatomic measurements in human larynges. Considering that the maximum muscle activation stress and its cross-sectional area and orientation are the most important factors in determining the effects of muscle activation, we can reasonably assume that our model captured the essential features of vocal fold posturing due to the LCA and TA activation, as demonstrated by the qualitative agreement with canine experimental observations. Similar inaccuracies due to lack of experimental data also existed on the geometry of the layered structure of the vocal folds and muscles. The uniform cross section shape of the vocal folds along the anterior–posterior direction is clearly a simplification of the more realistic geometry. However, vocal fold models of uniform cross-sectional geometry have been used in previous studies, both experimental and numerical [26–30,23,31], and have been shown to be able to reproduce some important features of phonation, including phonation frequency, aerodynamics, and vocal fold vibration pattern. Thus, this simplified geometry provides a reasonable starting point for modeling when reliable experimental data are inaccessible. Nevertheless, the conclusions of this study need to be verified in future studies when experimental data become available regarding material properties of the human larynx before it can be generalized to human phonation. Due to difficulties in experimental measurement of these properties, one future research direction of interest would be to conduct detailed sensitivity studies to investigate the influence of these material properties.

Besides using more realistic geometry and material properties, another direction of further improvement is to model the PCA and IA muscles as continuum structures instead of modeling their effects as point forces applied to the muscular process of the arytenoid cartilage. Modeling the muscle fiber deformation and how its orientation changes under muscle activation would allow a more realistic and accurate representation of the muscle force and thus its effect on vocal fold posturing. This is particularly the case for the IA muscle, activation of which is expected to play an important role in cartilaginous adduction of the vocal folds but was not investigated in this study. It is possible that activation of the IA muscle would allow complete adduction of the posterior glottis even in the presence of strong TA activation, which needs to be considered in future studies. In the long term, inclusion of all relevant laryngeal muscles would eventually allow us to predict consequences of muscular activation on vocal fold posturing and voice production in general.

Acknowledgment

This study was supported by Grant Nos. R01 DC011299 and R01 DC009229 from the National Institute on Deafness and Other Communication Disorders, the National Institutes of Health.

References

[1] Klatt, D. H., and Klatt, L. C., 1990, "Analysis, Synthesis and Perception of Voice Quality Variations Among Male and Female Talkers," J. Acoust. Soc. Am., **87**, pp. 820–856.
[2] Kreiman, J., and Sidtis, D., 2011, *Foundations of Voice Studies: An Interdisciplinary Approach to Voice Production and Perception*, Wiley-Blackwell, Hoboken, NJ.
[3] Zhang, Z., 2011, "Restraining Mechanisms in Regulating Glottal Closure During Phonation," J. Acoust. Soc. Am., **130**, pp. 4010–4019.
[4] Hirano, M., 1974, "Morphological Structure of the Vocal Fold and Its Variations," Folia Phoniatr., **26**(2), pp. 89–94.
[5] Hirano, M., and Kakita, Y., 1985, "Cover-Body Theory of Vocal Fold Vibration," *Speech Science: Recent Advances*, R. G. Daniloff, ed., College-Hill Press, San Diego, CA, pp. 1–46.
[6] Titze, I. R., and Talkin, D. T., 1979, "A Theoretical Study of the Effects of Various Laryngeal Configurations on the Acoustics of Phonation," J. Acoust. Soc. Am., **66**(1), pp. 60–74.
[7] van den Berg, J. W., and Tan, T. S., 1959, "Results of Experiments With Human Larynxes," Pract. Otorhinolaryngol., **21**, pp. 425–450.
[8] Bateman, H. E., and Mason, R. B., 1984, *Applied Anatomy and Physiology of the Speech and Hearing Mechanism*, Charles C Thomas, Springfield, IL.
[9] Chhetri, D., Neubauer, J., and Berry, D., 2012, "Neuromuscular Control of Fundamental Frequency and Glottal Posture at Phonation Onset," J. Acoust. Soc. Am., **131**(2), pp. 1401–1412.
[10] Choi, H., Berke, G., Ye, M., and Kreiman, J., 1993, "Function of the Thyroarytenoid Muscle in a Canine Laryngeal Model," Ann. Otol., Rhinol. Laryngol., **102**, pp. 769–776.
[11] Chen, T., Chodara, A. M., Sprecher, A. J., Fang, F., Song, W., Tao, C., and Jiang, J. J., 2012, "A New Method of Reconstructing the Human Laryngeal Architecture Using Micro-MRI," J. Voice, **26**(5), pp. 555–562.
[12] Kasperbauer, J. L., 1998, "A Biomechanical Study of the Human Cricoarytenoid Joint," Laryngoscope, **108**(11), pp. 1704–1711.
[13] Selbie, W. S., Zhang, L., Levine, W. S., and Ludlow, C. L., 1998, "Using Joint Geometry to Determine the Motion of the Cricoarytenoid Joint," J. Acoust. Am., **103**(2), pp. 1115–1127.
[14] Selbie, W. S., Gewalt, S. L., and Ludlow, C. L., 2002, "Developing an Anatomical Model of the Human Laryngeal Cartilages From Magnetic Resonance Imaging," J. Acoust. Soc. Am., **112**(3), pp. 1077–1090.
[15] Storck, C., Juergens, P., Fischer, C., Wolfensberger, M., Honegger, F., Sorantin, E., Friedrich, G., and Gugatschka, M., 2011, "Biomechanics of the Cricoarytenoid Joint: Three-Dimensional Imaging and Vector Analysis," J. Voice, **25**(4), pp. 406–410.
[16] Wang, R. C., 1998, "Three-Dimensional Analysis of Cricoarytenoid Joint Motion," Laryngoscope, **108**, pp. 1–17.
[17] Farley, G. R., 1996, "A Biomechanical Laryngeal Model of Voice F_0 and Glottal Width Control," J. Acoust. Soc. Am., **100**(6), pp. 3794–3812.
[18] Gommel, A., Butenweg, C., Bolender, K., and Grunendahl, A., 2007., "A Muscle Controlled Finite-Element Model of Laryngeal Abduction and Adduction," Comput. Method Biomec. Biomed. Eng., **10**(5), pp. 377–388.
[19] Hunter, E. J., Titze, I. R., and Alipour, F., 2004, "A Three-Dimensional Model of Vocal Fold Abduction/Adduction," J. Acoust. Soc. Am., **115**(4), pp. 1747–1759.
[20] Titze, I. R., and Hunter, E. J., 2007, "A Two-Dimensional Biomechanical Model of Vocal Fold Posturing," J. Acoust. Soc. Am., **121**(4), pp. 2254–2260.
[21] Hunter, E. J., and Thomson, S. L., 2012, "Solid CAD Models of Human Laryngeal Cartilage," Created From Selbie et al., National Repository for Laryngeal Data, Technical Note, No. 6, April 2002, Version 1.0.
[22] Ishizaka, K., 1981, "Equivalent Lumped-Mass Models of Vocal Fold Vibration," *Vocal Fold Physiology*, K. N. Stevens and M. Hirano, eds., University of Tokyo, Tokyo, Japan, pp. 231–244.
[23] Zhang, Z., 2009, "Characteristics of Phonation Onset in a Two-Layer Vocal Fold Model," J. Acoust. Soc. Am., **125**(2), pp. 1091–1102.
[24] Zhang, Z., 2014, "The Influence of Material Anisotropy on Vibration at Onset in a Three-Dimensional Vocal Fold Model," J. Acoust. Soc. Am., **135**(3), pp. 1480–1490.
[25] Zhang, Z., Neubauer, J., and Berry, D. A., 2007, "Physical Mechanisms of Phonation Onset: A Linear Stability Analysis of an Aeroelastic Continuum Model of Phonation," J. Acoust. Soc. Am., **122**(4), pp. 2279–2295.
[26] Becker, S., Kniesburges, S., Muller, S., Delgado, A., Link, G., Kaltenbacher, M., and Dollinger, M., 2009, "Flow-Structure-Acoustic Interaction in a Human Voice Model," J. Acoust. Soc. Am., **125**(3), pp. 1351–1361.
[27] Bhattacharya, P., and Siegmund, T., 2013, "A Computational Study of Systematic Hydration in Vocal Fold Collision," Comput. Methods Biomech. Biomed. Eng., **17**(16), pp. 1835–1852.

[28] Mendelsohn, A. H., and Zhang, Z., 2011, "Phonation Threshold Pressure and Onset Frequency in a Two-Layer Physical Model of the Vocal Folds," J. Acoust. Soc. Am., **130**(5), pp. 2961–2968.
[29] Pickup, B. A., and Thomson, S. L. 2009, "Influence of Asymmetric Stiffness on the Structural and Aerodynamic Response of Synthetic Vocal Fold Models," J. Biomech., **42**(14), pp. 2219–2225.
[30] Scherer, R., Shinwari, D., De Witt, K., Zhang, C., Kucinschi, B., and Afjeh, A., 2001, "Intraglottal Pressure Profiles for a Symmetric and Oblique Glottis With a Divergence Angle of 10 Degrees," J. Acoust. Soc. Am., **109**(4), pp. 1616–1630.
[31] Zheng, X., Bielamowicz, S., Luo, H., and Mittal, R., 2009, "A Computational Study of the Effect of False Vocal Folds on Glottal Flow and Vocal Fold Vibration During Phonation," Ann. Biomech. Eng., **37**(3), pp. 625–642.
[32] Eckel, H. E., and Sittel, C., 1995, "Morphometry of the Larynx in Horizontal Sections," Am. J. Otol., **16**(1), pp. 40–48.
[33] Mineck, C. W., Niro, T., Chan, R., and Titze, I. R., 2000, "Three-Dimensional Anatomic Characterization of the Canine Laryngeal Abduction and Adduction Musculature," Ann. Otol., Rhinol., Laryngol., **109**, pp. 505–513.
[34] Bol, M., and Reese, S., 2008, "Micromechanical Modeling of Skeletal Muscles Based on the Finite Element Method," Comput. Methods Biomech. Biomed. Eng., **11**(5), pp. 489–504.
[35] Grasa, J., Ramirez, A., Osta, R., Munoz, M., Soteras, F., and Calvo, B., 2011, "A 3D Active-Passive Numerical Skeletal Muscle Model Incorporating Initial Tissue Strains. Validation With Experimental Results on Rat Tibialis Anterior Muscle.," Biomech. Model. Mechanobiol., **10**(5), pp. 779–787.
[36] Yin, J., and Zhang, Z., 2013, "The Influence of Thyroarytenoid and Cricothyroid Muscle Activation on Vocal Fold Stiffness and Eigenfrequencies," J. Acoust. Soc. Am., **133**(5), pp. 2972–2983.
[37] Holzapfel, G. A., Gasser, T. C., and Ogden, R. W., 2000, "A New Constitutive Framework for Arterial Wall Mechanics and a Comparative Study of Material Models," J. Elasticity, **61**(1–3), pp. 1–48.
[38] Zhang, K., Siegmund, T., and Chan, R. W., 2007, "A Two-Layer Composite Model of the Vocal Fold Lamina Propria for Fundamental Frequency Regulation," J. Acoust. Soc. Am., **122**(2), pp. 1090–1101.
[39] Blemker, S. S., Pinsky, P. M., and Delp, S. L. 2005, "A 3D Model of Muscle Reveals the Causes of Nonuniform Strains in the Biceps Brachii," J. Biomech., **38**(4), pp. 657–665.
[40] Alipour-Haghighi, F., Titze, I. R., and Perlman, A. L., 1989, "Tetanic Contraction in Vocal Fold Muscle," J. Speech Hear Res., **32**, pp. 226–231.
[41] Berke, G., Mendelsohn, A., Howard, N., and Zhang, Z., 2013, "Neuromuscular Induced Phonation in a Human Ex Vivo Perfused Larynx Preparation," J. Acoust. Soc. Am., **133**(2), Paper No. EL114-EL117.
[42] Deguchi, S., Kawahara, Y., and Takahashi, S., 2011, "Cooperative Regulation of Vocal Fold Morphology and Stress by the Cricothyroid and Thyroarytenoid Muscles," J. Voice, **25**(6), pp. e255–e263.
[43] Chhetri, D., Berke, G., Lotfizadeh, A., Goodyer, E., 2009, "Control of Vocal Fold Cover Stiffness by Laryngeal Muscles: A Preliminary Study," Laryngoscope, **119**(1), pp. 222–227.
[44] Probst, K. X., Ybarra, M. A. S., Kashima, H., and Crosby, R. W., 2004, "Topography and Interactions of the Arytenoid and Cricoid Articular Facets: Implications for Vocal Process Positional Shifts," Clin. Anat., **17**(3), pp. 206–213.